ACES Asian Chemical Editorial Society

doi.org/10.1002/asia.202500835

CHEMISTRY
AN ASIAN JOURNAL
Research Article

www.chemasianj.org

Theoretical Study on Coordination Chemistry of Two Water-Soluble Ligands for Stripping Separation of Transplutonium Ions

Pin-Wen Huang,*[a] Peng Ren,[b] and Ming Qi[c]

Purification and mutual separation of trivalent actinides (An^{3+}: Am, Cm, Bk, Cf) present significant challenges in nuclear waste treatment. Elucidating complexation mechanisms with stripping ligands is crucial for ligand development. Given the radiotoxicity, quantum chemical methods are essential. This DFT study investigates chelation of An^{3+} ions with water-soluble ligands H_2L^{2py} and H_2L^{2pz}. Probable back-extraction complexes ($[AnL^{i}(H_2O)_j]^{+}$, $AnL^{i}(NO_3)(H_2O)^{k}$) exhibit near-identical geometries with minor An—O/N bond length variations. Analyses reveal enhanced chelating ability for diamine N atoms adjacent to carboxylate O versus *N*-heterocyclic donors (pyridine/pyrazine). Crucially, interaction intensity and partial covalency between An^{3+} and donor atoms (N_{AM}, O_{CA}, $N_{PY/PZ}$) display a distinct bimodal variation with Cm as the turning point. This trend likely originates from closer orbital energy matching between the 5f orbitals of Am/Bk/Cf and ligand 2p orbitals compared to Cm. Thermodynamic analyses demonstrate superior back-extraction ability for H_2L^{2py}, while H_2L^{2pz} excels in Am/Eu separation. The downward-upward trend in reaction free energies aligns with covalency variations, suggesting potential intra-group separation capability for all four ions. Estimated separation factors $SF_{Am/Cm}$, $SF_{Bk/Cm}$, and $SF_{Cf/Cm}$ are projected within 2.45–3.45.

1. Introduction

In recent decades, nuclear energy has witnessed renewed growth owing to its economic feasibility and reduced carbon emissions.[1,2] This resurgence, however, coincides with persistent challenges in managing spent nuclear fuels-a critical bottleneck for sustainable nuclear energy development.[3,4] The well-established PUREX process,[5] a renowned wet method, can effectively recycle almost all the plutonium and uranium isotopes. However, the residual liquid effluents from this process still contain transplutonium elements (such as Am, Cm, Bk, and Cf), which constitute the bulk of the radioactivity in PUREX liquid waste, alongside other fission products. To ensure long-term safety and minimize environmental contamination, these residual effluents require further purification. On the other hand, certain isotopes of transplutonium elements also hold considerable practical usages.[6,7] For example, ^{241}Am is utilized in ionization smoke detectors and, when combined with beryllium, it can also serve as a neutron source for various detection and material analysis applications. Similarly, ^{252}Cf is a highly valuable neutron source isotope due to its intense neutron emission, moderate half-life, and versatility. Therefore, the separation and recovery of transplutonium elements remain a critical and valuable endeavor in the field of nuclear science and technology. However, due to nearly identical chemical properties and ionic radii, mutual separation of trivalent americium (Am), curium (Cm), berkelium (Bk), and californium (Cf) ions presents a significant scientific challenge. Consequently, the design and synthesis of highly efficient extraction ligands for the intra group separation of Am, Cm, Bk, Cf have become a central focus of research in this field.[8,9]

Ideal ligands for intra-group actinide separation are either lipophilic extraction ligands with superior extraction preference toward special actinide ions or water-soluble back-extraction ligands with high back-extraction separation efficiency. In 2013, Y. Sasaki et al. found that using TEDGA as a masking agent, the lipophilic NTAamide(C_8) ligand could achieve separation of Am and Cm during the back-extraction process, with a maximum separation factor ($SF_{Cm/Am}$) of 6.5.[10,11] G. Modolo also discovered a synergistic extraction system composed of the neutral ligand $(ClPh)_2PSSH$ and the acidic tri(2-ethylhexyl) phosphate ligand (TEHP) exhibited highly effective separation of Am and Cm with the separation factor of 6∼10 under suitable conditions.[12] However, these ligand systems still possess some critical shortcomings: suboptimal separation performance, inadequate radiation resistance, and limited environmental sustainability.[13] Furthermore, the mechanism underlies their separation abilities also remain poorly understood, presenting a significant hinderance to their further optimization and usage.[14]

Theoretically, an in-depth investigation into the covalency disparities among transplutonium elements might facilitate their intra-group separation. Some recent works[15–18] also suggest the

[a] *P.-W. Huang*
Nanxun Innovation Institute, Zhejiang University of Water Resources and Electric Power, Hangzhou 310000, China
E-mail: ndhuangpw@gmail.com

[b] *P. Ren*
School of Nuclear Science and Technology, East China University of Technology, Nanchang 330013, China

[c] *M. Qi*
School of Physics, Nanjing University, Nanjing 210008, China

Supporting information for this article is available on the WWW under https://doi.org/10.1002/asia.202500835

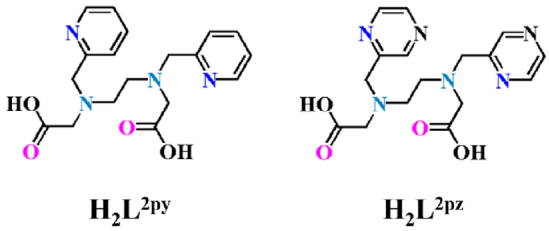

Figure 1. Structures of two studied back-extraction ligands (H_2L^{2py} and H_2L^{2pz}).

covalent character of bonds between trivalent transplutonium ions and donor N, O atoms exhibit distinct behaviors, differing not only from that of lanthanides but also from early actinides. Historically, chemists believed that early actinides, like thorium and uranium, would predominantly engage in covalent bonding because of their electronic configurations, while as the series progresses to heavier actinides, the effects of orbital contraction were predicted to result in a shift toward predominantly ionic bonding behavior, thus the covalence between transplutonium ions and donor nitrogen or oxygen atoms may decrease along Am, Cm, Bk, Cf.[14,19,20] Nevertheless, in 2014, with the synthesized of californium borate ($Cf[B_6O_8(OH)_5]$) by Polinski,[21] unexpected high covalent character was observed in Cf-O bond. Then in 2015, Thomas E. Albrecht-Schmitt also found covalent character exist in Cf-O and Cf-N bonds of$[Cf(DPA)_3]^{3-}$ complex.[22] Through density functional theory method, Shi and colleagues[23] studied the interactions between phenanthroline-derived bis-triazine ligands and Am, Cm, Bk, Cf, they found that interaction intensity between transplutonium atoms and N donor atoms decrease along Am, Cm, Bk, Cf, while the covalency descriptors (such as energy density of electrons (H) and the ratio between absolute potential energy density and kinetic energy (|V|/G) at bond critical point) suggest that covalency "break" in Cf. In 2021 and 2022, Kaltsoyannis's theoretical works[24,25] about $AnCl_3$ and $AnCl_2$ indicating that energy degeneracy covalence increases moderately in the second half series of actinides, and the turning point is Bk. However, in another theoretical work about the interaction between transplutionium atoms and crown ethers,[26] the intensity and covalency seem to decreases along Am, Cm, Bk, Cf, no covalent break phenomenon was found in these four actinide crown ether complexes. Therefore, whether this covalency break exist, and at which point break also remain an open and interesting question, thus deserve in-depth investigation.[27]

In 2015, S. Gracia and collaborators[28] found the water-soluble ligand *N,N,N′,N″*-tetrakis(6- carboxy-2-pyridylmethyl) ethylenediamine (H_4TPAEN) can be used for the back-extraction separation of trivalent Am and Cm ions, with a back-extraction separation factor of 3.5. However, this water-soluble ligand is fragile to protonation and has very low solubility in water (smaller than 0.05 mmol/L).[29,30] Heitzmann and collaborators[31] then developed two analogous molecules of H_4TPAEN with better water-solubility, *N,N*-bis(2- pyridinyl-methyl) ethylenediamine *N′,N′*-di-acetic acid (Figure 1, short as H_2L^{2py}) and *N,N*-bis(2-pyrazyl-methyl) ethylenediamine *N′,N′*-di-acetic acid (Figure 1, short as H_2L^{2pz}). For H_2L^{2py}, four carboxylic pyridine rings of H_4TPAEN were replaced by two carboxylic acid groups and two pyridine rings, while for H_2L^{2pz}, carboxylic pyridine rings were replaced by two carboxylic acid groups and two pyrazine rings. Both H_2L^{2py} and H_2L^{2pz} possess striping separation ability between Am^{3+} and Eu^{3+}, and they also have better water solubility compared to H_4TPAEN. Now, there are already a lot of experimental works[32,33] about these two ligands' extraction ability toward Am^{3+} and Eu^{3+}, less attention has been paid to their potential application in transplutonium element separation. We systematically explored the complexation of four transplutonium actinides (Am, Cm, Bk, Cf) with H_2L^{2py} and H_2L^{2pz} by quasi-relativistic density functional theory (DFT). In fact, both ligands possess two carboxylate oxygen atoms (O_{CA}), two diamine nitrogen atoms (N_{AM}), and two *N*-heterocyclic nitrogen atoms ($N_{PY/PZ}$), thus also forming ideal platforms to study the relationship between ligand's back-extraction separation ability and relative chelating ability of different types of donor atoms. In this work, we also conducted a detailed investigation into the geometric configurations and bonding characteristics of the back-extraction complexes, as well as the stripping efficiency of H_2L^{2py} and H_2L^{2pz} toward trivalent Am, Cm, Bk, Cf ions and lanthanide ion Eu^{3+}. This study can elucidate the coordination mechanism between H_2L^{2py}, H_2L^{2pz} and four transplutonium actinide elements, while also contributing to further development of related back-extraction ligands.

2. Computational Details

To model the aqueous-organic back-extraction process, ligand structures were first optimized in aqueous solution. For $An—L^{2py}$ and $An—L^{2pz}$ complexes, central actinide ions in aqueous solution consistently exhibit varying coordination numbers (CN = 6–12), with CN = 8,9, and 10 representing the most stable configurations.[34,35] Therefore, several actinide complexes of two ligands with coordination number 8, 9, and 10 including $[ML^i(H_2O)_2]^+$, $M(L^i)NO_3$, $[M(L^i)(H_2O)_3]^+$, $M(L^i)(NO_3)(H_2O)$, $[M(L^i)(H_2O)_4]^+$, $M(L^i)(NO_3)(H_2O)_2$ (M = Am, Cm, Bk, Cf, and Eu, $L^i = L^{2py}$ and L^{2pz}, respectively) were studied in this work. These metal complexes were optimized in water using the Gaussian 09 D.01[36] software package. The M06-L functional was employed throughout all the calculations of this work due to its demonstrated capability to accurately reproduce geometrical structures of Eu, Gd, and Sm complexes with ethylene-diaminetetraacetic acid (EDTA, a widely employed hexadentate benchmark ligand sharing three critical features with H_2L^{2py}/H_2L^{2pz}: analogous geometry, identical diamine backbone, and equivalent donor atom count, see Figure S1).[37,38] As presented in Table S1, the M06-L/6–31 + G(d)//ECP method achieves highly accurate $Ln—N_{AM}$ and $Ln—O_{CA}$ bond lengths with relative errors < 3.3%. Furthermore, M06-L incorporates some parameters fitted to non-covalent interaction energies,[39] enabling reliable acquisition of thermodynamic data for targeted back-extraction reactions. This capability is corroborated by collaborative theoretical studies,[40–42] which consistently demonstrate M06-L's proficiency in delivering reliable reaction free energies for actinide extraction/back-extraction systems at moderate computational cost.

In this work, the inner-core electrons of four transplutonium actinides (Am, Cm, Bk, Cf), and Eu were treated by the Stuttgart-Cologne groups' quasi-relativistic pseudo-potentials. Specifically, the ECP60MWB for four actinides and ECP28MWB for Eu. For the remained outer electrons, the segmental basis sets ECP60MWB-SEG for actinides and ECP28MWB-SEG for Eu were used.[43,44] For, Am^{3+}, Cm^{3+}, Bk^{3+}, Cf^{3+}, Eu^{3+}species, after preliminary test, the septet ($5f^6$), octet ($5f^7$), septet($5f^6$), sextet($5f^5$), and septet ($4f^7$) spin states were found to possess lowest electronic energies, thus were considered to be the ground states for studied complexes, respectively. To investigate the nature of interactions between transplutonium atoms (Am, Cm, Bk, Cf) and the N_{AM}, N_{PY}, N_{PZ}, and O_{CA} atoms of the studied molecules, Mayer's bond order (MBO) analysis was performed using Multiwfn 3.7.[45,46] Subsequently, Bader's quantum theory of atoms in molecules (QTAIM) and partial density of state (PDOS) analysis was conducted on the studied bonds using the same software. To obtain higher-accuracy thermodynamic data (Gibbs free energy, G_{sol}) for studied species in solution, we employed the larger basis set 6–311 + G(2df,p) for C, N, O, and H atoms during single-point energy calculations, conducted on structures pre-optimized at the M06-L/6–31 + G(d)/RECP level. Specifically, the G_{sol} energies were computed through comprehensive incorporation of: 1) thermal corrections (G_{corr}) derived from solvent-phase frequency calculations at the optimization theory level, 2) zero-point correction (ZPE), and 3) the $RT\ln RT/p$ term (1.89 kcal/mol), all applied to electronic energies obtained at the M06-L/6–311 + G(2df, p)/RECP theory level. The details of the Gibbs free energy calculations in solution is also shown in Figure S2. In some standard advanced wet processes (e.g., DIAMEX-SANEX, EXAm), combinations of organic ligands such as DMDOHEMA and HDEHP are used to co-extract actinide and lanthanide ions into total petroleum hydrocarbons (TPH). Performing quantum chemical calculations in such mixed-solvent environments presents significant challenges. To simplify the model, we selected *n*-dodecane (ε = 2.015), a primary constituent of TPH that is also widely employed in experimental studies within wet nuclear waste treatment, as a representative model system for TPH. The solvent effects for both aqueous and organic phases (*n*-dodecane) were incorporated via the Integral Equation Formalism Polarizable Continuum Model (IEFPCM),[47,48] widely recognized as an effective approach extensively validated in actinide solution chemistry.

3. Results and Discussions

3.1. Geometrical Structure and Electronic Properties of Studied Ligands

As weak acids, the ligands H_2L^{2py} and H_2L^{2pz} undergo partial deprotonation to form $[HL^{2py}]^-$ and $[HL^{2pz}]^-$ ions in aqueous solution. Consequently, both neutral ligands and their monoanionic forms were structurally optimized within the aqueous phase. To investigate ligands' affinity for Am^{3+}, Cm^{3+}, Bk^{3+}, Cf^{3+} and Eu^{3+} ions, electrostatic potential (ESP) of studied ligands were analyzed utilizing GaussView 6.0 and Multiwfn 3.7. The optimized geometrical structures and electrostatic potential (ESP) maps of the studied ligands are presented in Figure 2. Corresponding quantitative descriptors including the minimum ESP values proximal to each of the three types of donor atoms, Hirshfeld atomic charges, and atomic dipole moment-corrected Hirshfeld charges (ADCH)[49] are systematically summarized in Table 1.

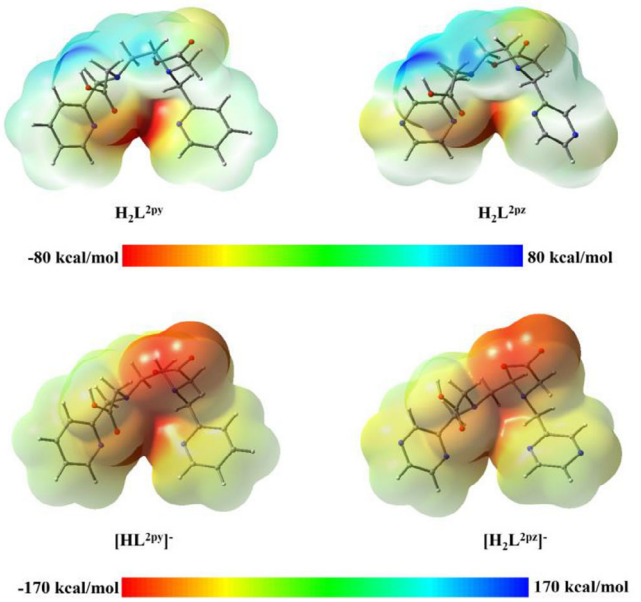

Figure 2. The ESP maps of the investigated ligands computed at the M06-L/6–311 + G(2df,p) level.

After optimization, both ligands adopt capsule-shaped cavities (Figure 2). Their hexadentate binding frameworks enable precise positioning of actinide ions within the cavity center. Figure 2 further reveals the most negative electrostatic potential regions (deepest red) localized near: 1) carboxylic oxygen atoms (O_{CA}), and 2) pyridine/pyrazine nitrogen atoms ($N_{PY/NPZ}$) in neutral ligands. This spatial distribution strongly indicates that N_{PY}, N_{PZ}, and O_{CA} atoms function as primary electron-donating sites. Systematic analysis reveals higher atomic charges and more negative electrostatic potential (ESP) values at donor atoms (N_{PY}, N_{AM}, and O_{CA} atoms) of H_2L^{2py}($[HL^{2py}]^-$) relative to corresponding sites (N_{PZ}, N_{AM}, O_{CA}) in H_2L^{2pz}/$[HL^{2pz}]^-$. This electronic structure disparity consistently correlates with H_2L^{2py}'s superior chelating affinity and thermodynamic back-extraction capability, ultimately corroborating its enhanced chelating performance over H_2L^{2pz}. As further illustrated in Figure 2, deprotonation of carboxylic groups induces a migration of the most negative ESP region toward the diamine backbone. Concomitantly, electrostatic potentials at all three types of donor atoms become significantly more negative. Notably, despite exhibiting lower atomic charges relative to $N_{PY/PZ}$ and O_{CA} atoms, N_{AM} atoms demonstrate nearly comparable ESP values, revealing their substantial electron-donating capability. Consequently, these diamine nitrogen atoms (N_{AM}) may play very important roles in mediating back-extraction efficiency and separation selectivity, and crucially dictating the overall performance of the studied ligands.

Table 1. Calculated Hirshfeld and ADCH charges as well as ESP values at donor atoms of the neutral H_2L^{2py} and H_2L^{2pz} and the deprotonated ligands $[HL^{2py}]^-$ and $[HL^{2pz}]^-$.[a)]

	$H_2L^{2py}/[HL^{2py}]^-$			$H_2L^{2pz}/[HL^{2pz}]^-$		
	N_{AM}	N_{PY}	O_{CA}	N_{AM}	N_{PZ}	O_{CA}
Hirshfeld charge (e)	−0.094/−0.098	−0.183/−0.186	−0.231/−0.372	−0.089/−0.097	−0.149/−0.157	−0.228/−0.368
ADCH (e)	−0.260/−0.255	−0.327/−0.301	−0.355/−0.587	−0.244/−0.256	−0.296/−0.261	−0.314/−0.583
[b)]ESP value (kcal/mol)	−52.64/−160.41	−78.16/−162.97	−78.28/−163.69	−58.83/−147.35	−66.67/−148.59	−66.84/−153.81

[a)] …/…represents the results of related data in neutral ligands (H_2L^i) and its deprotonated ligands ($[HL^i]^-$), respectively (L^i = L^{2py} and L^{2pz}). [b)] Obtained at the local minimum point of ESP nearest to the studied donor atom.

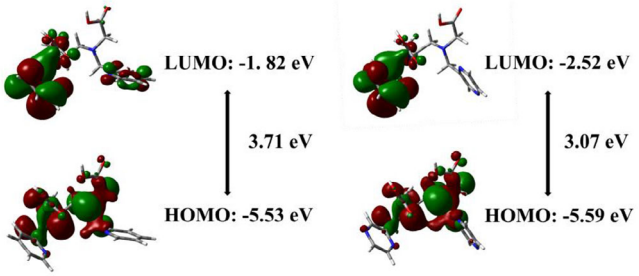

Figure 3. HOMO and LUMO orbitals of ligands H_2L^{2py} (left) and H_2L^{2pz} (right), along with their corresponding molecular orbital energies (eV), computed at the M06-L/6–311 + G(2df,p) level. (Isosurface value = 0.02 a.u.).

Molecular orbitals of the ligands were computed at the M06-L/6–311 + G(2df,p) level using aqueous-optimized structures. The highest occupied (HOMO) and lowest unoccupied (LUMO) molecular orbitals for H_2L^{2py} and H_2L^{2pz} are presented in Figure 3. Orbital analysis reveals that HOMO electron density in both ligands is predominantly localized on O_{CA} and N_{AM} atoms within the diamine-carboxylate backbone. Notably, the LUMO of H_2L^{2py} exhibits spatial distribution centered on both pyridine rings and one N_{AM} atom, whereas H_2L^{2pz}'s LUMO is primarily delocalized over a single pyrazine ring and adjacent N_{AM} atom. Consequently, N_{AM} atoms in H_2L^{2pz} may demonstrate a significantly enhanced contribution to back-extraction reactions compared to those in H_2L^{2py}. This mechanistic distinction correlates with H_2L^{2pz}'s reduced HOMO-LUMO gap (3.07 eV versus 3.73 eV for H_2L^{2py}), quantitatively supporting its superior electronic reactivity.

3.2. Structures of the An—L^{2py} and An—L^{2pz} Complexes

Generally, in practical wet-method nuclear waste treatment processes utilizing the studied back-extraction ligands, the minor actinides and other fission products (like lanthanides) are first co-extracted from an acid solution into an organic solution with hydrophobic ligands, such as the DEMOHEDA and HEDHP ligand combination. Subsequently, the studied target ions (Am^{3+}, Cm^{3+}, Bk^{3+}, Cf^{3+}) can be selectively stripped from the organic to the aqueous phase by H_2L^{2py} and H_2L^{2pz} employed as stripping agents. In this work, metal complexes $ML^i(NO_3)$, $[ML^i(H_2O)_2]^+$, $ML^i(NO_3)(H_2O)$, $[ML^i(H_2O)_3]^+$, $ML^i(NO_3)(H_2O)_2$, and $[ML^i(H_2O)_4]^+$ (M = Am, Cm, Bk, Cf, and Eu; L^i = L^{2py} and L^{2pz}) were selected to represent the probable back-extraction products of these two water-soluble ligands. We also optimized the related Eu-complexes as control systems. All geometrical structures of the aforementioned ligands and metal complexes were optimized in aqueous solution without symmetry restriction at the M06-L/6–31 + G(d)/RECP level of theory. As representative examples, the optimized geometries of the $ML^i(NO_3)(H_2O)$ complexes (M = Am, Cm, Bk, Cf, and Eu; L^i = L^{2py} and L^{2pz}, respectively), exhibiting no imaginary frequencies, are presented in Figure 4. The optimized geometries of other studied actinide complexes including $[ML^i(H_2O)_2]^+$, $[ML^i(H_2O)_3]^+$, $[ML^i(H_2O)_4]^+$, $ML^i(NO_3)$, and $ML^i(NO_3)(H_2O)_2$ (M = Am, Cm, Bk, Cf, Eu; L^i = L^{2py} and L^{2pz}) are presented in Figures S3-1 to S3-5.

As presented in Figure 4, the representative metal complexes ($ML^i(NO_3)(H_2O)$ (M = Am, Cm, Bk, Cf, Eu; L^i = L^{2py}, L^{2pz})) for the four trivalent actinide ions and Eu exhibit nearly identical geometrical structures. Slight differences exist only in the twist angles of the side *N*-heterocyclic rings. The calculated bond lengths for $ML^i(NO_3)(H_2O)$ and other studied complexes are presented in Table 2 ($ML^i(NO_3)(H_2O)$) and Table S2 (other complexes). Notably, all calculated Eu—$N_{AM/PY/PZ}$ bond lengths in the model complexes are slightly shorter than Am—$N_{AM/PY/PZ}$ counterparts, contradicting the fact that both ligands exhibit superior chelating (and selective stripping) ability toward Am^{3+} ions. In fact, numerous theoretical studies[50,51] have demonstrated that bond lengths (interatomic distances) may inadequately reflect the strength of interactions between actinides and donor N/O atoms. An alternative metric, termed the "effective bond length" (denoted d_{eff}(M—N/O)), which subtracts the ionic radius of the central metal ion from the interatomic distance, may provide a more accurate representation of the bond strength. Here, the ionic radii of the studied transplutonium ions were obtained from literature[52] (Am^{3+}: 0.97 Å, Cm^{3+}: 0.97 Å, Bk^{3+}: 0.96 Å, Cf^{3+}: 0.95 Å, and Eu^{3+}: 0.95 Å). Using these values, we calculated the aforementioned effective bond lengths (d_{eff}) for the studied bonds, which are also listed in Tables 2 and S2. The variation in d_{eff} across the Am, Cm, Bk, and Cf series is presented in Figures S4-1 to S4-4. Analysis of these tables and figures reveals that all d_{eff} (Am—N/O) values are smaller than their corresponding d_{eff}(Eu—N/O) values in the analogous complexes.

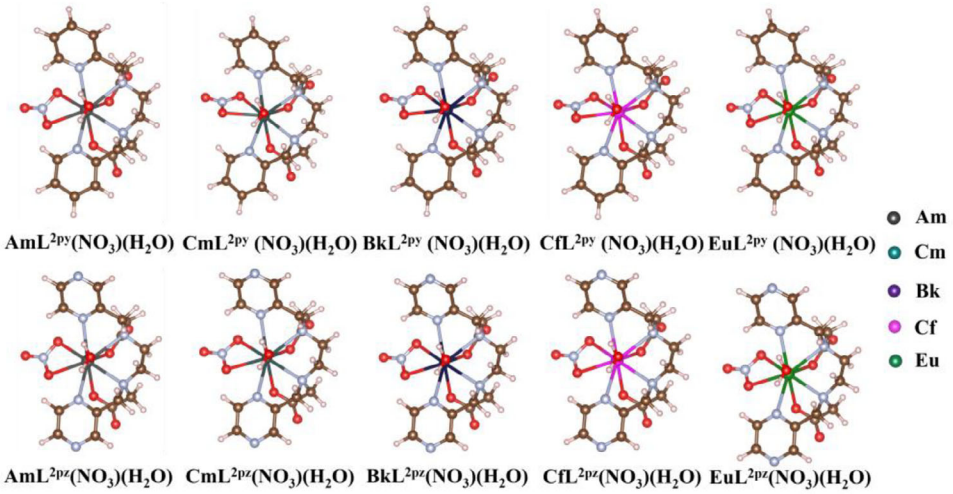

Figure 4. Optimized geometries of M-complexes $M(L^i)(NO_3)(H_2O)$ (M = Am, Cm, Bk, Cf, Eu; $L^i = L^{2py}$, L^{2pz}) in aqueous solution.

Table 2. Average M—N_{AM}, M—$N_{PY/PZ}$, M—O_{CA} bond distances and effective bond lengths (Å) for investigated $An(L^i)(NO_3)(H_2O)$ and $[An(L^i)(H_2O)_3]^+$ complexes (L^i=L^{2py}/L^{2pz}) at the M06-L/6–31 + G(d)/RECP level.

Complexes	Bond length (M—N_{AM})	d_{eff}(M—N_{AM})	Bond length (M—$N_{PY/PZ}$)	d_{eff}(M—$N_{PY/PZ}$)	Bond length (M—O_{CA})	d_{eff}(M—O_{CA})
$AmL^i(NO_3)(H_2O)$	2.693/2.710	1.713/1.730	2.770/2.788	1.790/1.808	2.398/2.395	1.418/1.415
$CmL^i(NO_3)(H_2O)$	2.685/2.712	1.715/1.742	2.758/2.802	1.788/1.832	2.399/2.383	1.429/1.413
$BkL^i(NO_3)(H_2O)$	2.655/2.691	1.695/1.731	2.766/2.765	1.806/1.805	2.356/2.356	1.396/1.396
$CfL^i(NO_3)(H_2O)$	2.629/2.673	1.679/1.723	2.746/2.747	1.796/1.797	2.324/2.329	1.374/1.379
$EuL^i(NO_3)(H_2O)$	2.676/2.682	1.726/1.732	2.756/2.771	1.806/1.821	2.376/2.370	1.426/1.420
$[AmL^i(H_2O)_3]^+$	2.707/2.719	1.727/1.739	2.787/2.802	1.807/1.822	2.395/2.382	1.415/1.402
$[CmL^i(H_2O)_3]^+$	2.708/2.722	1.738/1.752	2.791/2.823	1.821/1.853	2.401/2.407	1.431/1.437
$[BkL^i(H_2O)_3]^+$	2.669/2.693	1.709/1.733	2.765/2.793	1.805/1.833	2.371/2.360	1.411/1.400
$[CfL^i(H_2O)_3]^+$	2.652/2.663	1.702/1.713	2.745/2.758	1.795/1.808	2.333/2.327	1.383/1.377
$[EuL^i(H_2O)_3]^+$	2.704/2.715	1.754/1.765	2.766/2.780	1.816/1.830	2.386/2.373	1.436/1.423

[a] …/…represents the results with $L^i = L^{2py}$ and L^{2pz}, respectively.

Analysis of Figure 5 and Figures S4-1 to S4-4 reveals that all d_{eff} (An—N_{AM}) values and most d_{eff} (An—$N_{PY/PZ}$) and d_{eff} (An—O_{CA}) values exhibit an "increase-decrease" trend across the Am, Cm, Bk, Cf series. Consequently, the strength of the corresponding An—N_{AM} bonds may follow a complementary "decrease-increase" pattern, with the breakpoint occurring at Cm. For An—$N_{PY/PZ}$ and An—O_{CA} bonds in most complexes, d_{eff} also exhibits this "increase-decrease" trend behavior. However, with the nitrate ion coordinate to the complexes, in $AnL^{2py}(NO_3)(H_2O)$, d_{eff}(An—N_{PY}) no longer follows this increasing-decreasing trend. For $AnL^i(NO_3)$ and $AnL^i(NO_3)(H_2O)_2$, more irregular trends are observed in d_{eff}(An—$N_{PY/PZ}$) and d_{eff}(An—O_{CA}) across the Am, Cm, Bk, Cf series, demonstrating the perturbation by the nitrated ions on the $N_{PY/PZ}$ and O_{CA} donor atoms. Consistently, the d_{eff} values for M—N/O bonds in M-L^{2py} complexes are shorter than those of corresponding bonds in M-L^{2pz} complexes, again indicating that H_2L^{2py} exhibits superior stripping ability compared to H_2L^{2pz}.

3.3. Bonding Nature Analyses

The bond strength between central metal ions and donor atoms (N, O) has been investigated using Mayer bond order (MBO) calculations at the M06-L/6–311 + G(2df,p)/RECP level of theory. The MBO values for the M—N_{AM}, M—$N_{PY/PZ}$, M—O_{CA} bonds in two representative CN = 9 model complexes ($ML^i(NO_3)(H_2O)$, $[ML^i(H_2O)_3]^+$, M = Am, Cm, Bk, Cf, Eu, $L^i = L^{2py}$, L^{2pz}) are presented in Table 3. MBO data for other studied complexes are listed in Table S4. Mayer bond order (MBO) analyses of $[AnL^i(H_2O)_2]^+$, $[AnL^i(H_2O)_3]^+$, and $[AnL^i(H_2O)_4]^+$ (An = Am, Cm, Bk, Cf; $L^i = L^{2py}$ and L^{2pz}) reveal that the strength of An—N_{AM}, An—$N_{PY/PZ}$, and An—O_{CA} bonds systematically decreases from Am to Cm, increases from Cm to Bk, and continues to increase from Bk to Cf. However, this characteristic decrease-increase trend is absent for An—N_{Pz}, and An—O_{CA} in nitrate-coordinated complexes such as $AnL^{2pz}(NO_3)(H_2O)$, $AnL^i(NO_3)$, and $AnL^i(NO_3)(H_2O)_2$. In $AnL^{2pz}(NO_3)(H_2O)_2$ complexes, the MBOs even

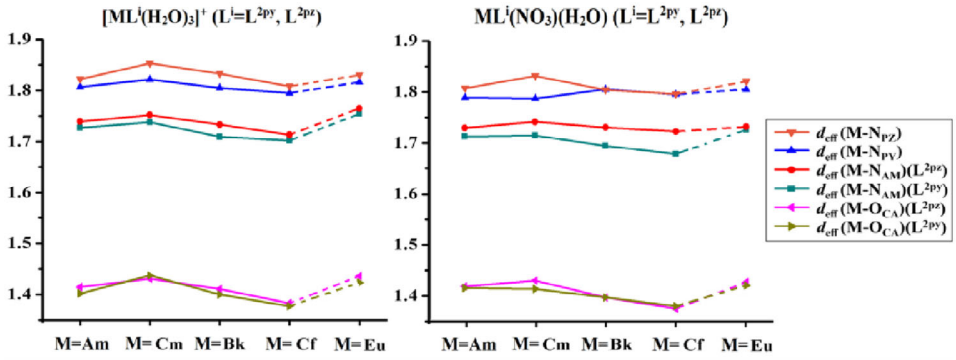

Figure 5. Trends in calculated effective bond lengths (d_{eff}) of M—N_{AM}, M—O_{CA}, M—$N_{PY/PZ}$ bonds for [ML^i(H$_2$O)$_3$]$^+$ complexes (left) versus ML^i(NO$_3$)(H$_2$O) complexes (right).

Table 3. Mayer bond orders of M—N_{AM}, M—$N_{PY/PZ}$, and M—O_{CA} bonds in investigated ML^i(NO$_3$)(H$_2$O) and [ML^i(H$_2$O)$_3$]$^+$ complexes.

Species	Mayer bond order		
	M—N_{AM}	M—$N_{PY/PZ}$	M—O_{CA}
Am(L^i)(NO$_3$)(H$_2$O)	0.350/0.335	0.177/0.183	0.353/0.360
Cm(L^i)(NO$_3$)(H$_2$O)	0.346/0.327	0.181/0.175	0.342/0.360
Bk(L^i)(NO$_3$)(H$_2$O)	0.359/0.331	0.159/0.175	0.357/0.368
Cf(L^i)(NO$_3$)(H$_2$O)	0.388/0.344	0.150/0.181	0.370/0.385
Eu(L^i)(NO$_3$)(H$_2$O)	0.286/0.284	0.199/0.197	0.386/0.391
[Am(L^i)(H$_2$O)$_3$]$^+$	0.340/0.329	0.185/0.195	0.370/0.378
[Cm(L^i)(H$_2$O)$_3$]$^+$	0.333/0.322	0.185/0.179	0.359/0.363
[Bk(L^i)(H$_2$O)$_3$]$^+$	0.353/0.334	0.182/0.191	0.378/0.385
[Cf(L^i)(H$_2$O)$_3$]$^+$	0.361/0.350	0.197/0.197	0.361/0.402
[Eu(L^i)(H$_2$O)$_3$]$^+$	0.281/0.150	0.206/0.187	0.363/0.378

[a] …/…represents the results with L^i = L^{2py} and L^{2pz}, respectively.

exhibit a reverse increase-decrease pattern. These observations again demonstrate that the nitrate counterion perturbs the metal ion affinity of N_{PY}/N_{PZ} and O_{CA} atoms, whereas the binding strength variation at N_{AM} sites consistently follows the decrease-increase trend across all studied complexes. Consequently, N_{AM} atoms may play pivotal roles in governing the metal ion selectivity of both ligands.

To further investigate the covalent character of interactions between actinide ions and the two ligands, key quantum theory of atoms in molecules (QTAIM) descriptors, including electron density (ρ), electronic energy density (H), and the absolute ratio of potential energy density to Lagrangian kinetic energy (|V|/G)[52,53] were computed at bond critical points (BCPs) of M—N_{AM}, M—$N_{PY/PZ}$ as well as M—O_{CA} bonds in the studied metal complexes using Multiwfn 3.7. These results are presented in Table S3.

From Table S3, all studied bonds in ML^i(NO$_3$)(H$_2$O) complexes exhibit positive $\nabla^2\rho$, while ρ values at their BCPs are below 0.2, indicating these bonds should be classified as closed-shell interactions. However, negative H values are observed for An—N_{AM} and An—O_{CA} bonds in AnL^i(NO$_3$)(H$_2$O) complexes. According to E. Espinosa's classification method,[54,55] these bonds exhibit partial covalent character (dative bonding). In contrast, all H values for Eu—N_{AM}, Eu—O_{CA} bonds are positive, indicating no partial covalent component in the corresponding bonds. Consequently, the preferential binding of actinide ions by both water-soluble ligands may originate from differential covalency character in An—N_{AM}/O_{CA} and Eu—N_{AM} /O_{CA}. This conclusion can also be drawn from the |V|/G values. Theoretically, $1 < |V|/G < 1.2$ serves as key evidence for partial covalent character in the associated bonds. In contrast to previous theoretical studies[56,57] on hydrophobic extraction ligands, no indications of partial covalency (negative H and $|V|/G > 1.0$) are observed in actinide ion interactions with $N_{PY/PZ}$ donor atoms. As established in the preceding discussion and prior work,[33] deprotonated O_{CA} significantly enhances the binding affinity of proximal N_{AM} atoms. This electronic effect subsequently modifies the electrostatic potential (ESP) distribution across the ligand framework, ultimately weakening the binding affinity of $N_{PY/PZ}$ donor atoms in both water-soluble ligands. The characteristic decrease-increase trend across Am, Cm, Bk, Cf is also evident in the H and |V|/G values for An—N_{AM} bonds, consistent with the above MBO analysis. This agreement further confirms distinct covalency variation at the Cm position. We propose this unique covalency progression may facilitate sequential separation of Am, Cm, Bk, and Cf. Moreover, M—N/O bonds systematically exhibit more negative H values (and larger |V|/G) in M-L^{2py} complexes than in M-L^{2pz} analogues. This observation confirms the superior chelating ability of H_2L^{2py} relative to H_2L^{2pz}. This covalency trend was further investigated via delocalization index (DI) analysis. DI, a quantitative metric denoting electron sharing between central atoms and donors,[58] provides enhanced characterization of covalent interactions. Using Multiwfn 3.7′s basin analysis tool, we calculated DIs for relevant bonds in ML^i(NO$_3$)(H$_2$O) and [ML^i(H$_2$O)$_3$]$^+$ complexes. Table 4 confirms the partial covalent character of An—N_{AM} and most An—O_{CA}, An—$N_{PY/PZ}$ bonds follow a decrease-increase progression with a transition at Cm. Consequently, the An—N_{AM} trend originates from electron-sharing covalent character between actinides and N_{AM}, $N_{PY/PZ}$, O_{CA} donor atoms.

The partial density of states (PDOS) for the AnL^{2pz}(NO$_3$)(H$_2$O) complexes are plotted in Figures 6. Five fragments including 5*f*,

Table 4. Delocalization indexes (DIs) of M—N_{AM}, M—$N_{PY/PZ}$, and M—O_{CA} bonds in studied $ML^i(NO_3)(H_2O)$ and $[ML^i(H_2O)_3]^+$ complexes.

Species	DIs		
	M—N_{AM}	M—$N_{PY/PZ}$	M—O_{CA}
$Am(L^i)(NO_3)(H_2O)$	0.241/0.235	0.194/0.182	0.370/0.373
$Cm(L^i)(NO_3)(H_2O)$	0.223/0.212	0.185/0.165	0.345/0.358
$Bk(L^i)(NO_3)(H_2O)$	0.232/0.218	0.179/0.174	0.376/0.376
$Cf(L^i)(NO_3)(H_2O)$	0.239/0.220	0.185/0.177	0.387/0.388
$Eu(L^i)(NO_3)(H_2O)$	0.216/0.212	0.161/0.151	0.331/0.334
$[Am(L^i)(H_2O)_3]^+$	0.241/0.236	0.190/0.179	0.380/0.390
$[Cm(L^i)(H_2O)_3]^+$	0.219/0.212	0.172/0.158	0.342/0.333
$[Bk(L^i)(H_2O)_3]^+$	0.233/0.225	0.179/0.165	0.362/0.373
$[Cf(L^i)(H_2O)_3]^+$	0.233/0.230	0.207/0.174	0.378/0.391
$[Eu(L^i)(H_2O)_3]^+$	0.210/0.205	0.160/0.148	0.338/0.345

[a] …/…represents the results with $L^i = L^{2py}$ and L^{2pz}, respectively.

6d orbitals of the Am^{3+}, Cm^{3+}, Bk^{3+}, Cf^{3+} ions, and the 2*p* orbitals of the donor N_{AM}, $N_{PZ/PY}$, and O_{CA} atoms from both $[L^{2pz}]^{2-}$ and $[L^{2py}]^{2-}$ are defined. Notably, the HOMO energy level corresponding to the $AmL^{2pz}(NO_3)(H_2O)$ is energetically the lowest among the four actinide complexes, with Am-5f orbitals positioned closest to the corresponding molecule' HOMO level. Consequently, Am-5f orbitals demonstrate the strongest contribution to Am-ligand binding compared to other three actinide complexes. Furthermore, orbital overlap between An—5*f* and O_{CA}-2*p*, N_{AM}-2*p* orbitals progressively increases across the Cm-Bk-Cf series. These enhanced overlaps (Am-5*f*/Bk-5*f*/Cf-5*f* with N_{AM}-2*p*, O_{CA}-2*p*) may attribute to more energy degeneracy-driven covalent interactions relative to Cm-5*f* systems, ultimately causing the distinctive downward-upward partial covalency variation along Am-Cm-Bk-Cf sequence.

3.4. Thermodynamic Analysis

The back-extraction reaction occurring near the aqueous-organic interface constitutes an extremely complex multi-step process. It typically involves: 1) ligand transport from aqueous phase to interface, 2) dissociation of metal complexes within the organic phase, 3) formation of new complexes at the interface, and 4) transfer of these complexes into the aqueous phase. Prior to back-extraction, co-extraction of actinide and lanthanide cations from acidic aqueous solution into organic diluent is performed using extractant ligands. In processes such as EXAm, DIAMEX-SANEX, and certain GANEX operations,[59–61] the DMDOHEMA/HDEHP ligand combination co-extracts metal ions into TPH diluent. For this ligand system, multiple metal complex species coexist in the organic phase. Based on experimental and theoretical studies,[62,63] the predominant species is likely the $M(DEHP)_3(HDEHP)_2DMDOHEMA$ adducts. These large molecules contain over 400 atoms, largely due to their extensive and flexible alkyl chains. This high atom count renders their computational optimization extremely challenging. To save computational time and cost, many prior theoretical investigations have employed a simplification strategy, used the "alkyl chain truncation" method,[64–66] wherein the long alkyl chains in these complexes are replaced with shorter analogues to facilitate modeling. In the present work, we also used this alkyl chain truncation method, the structures

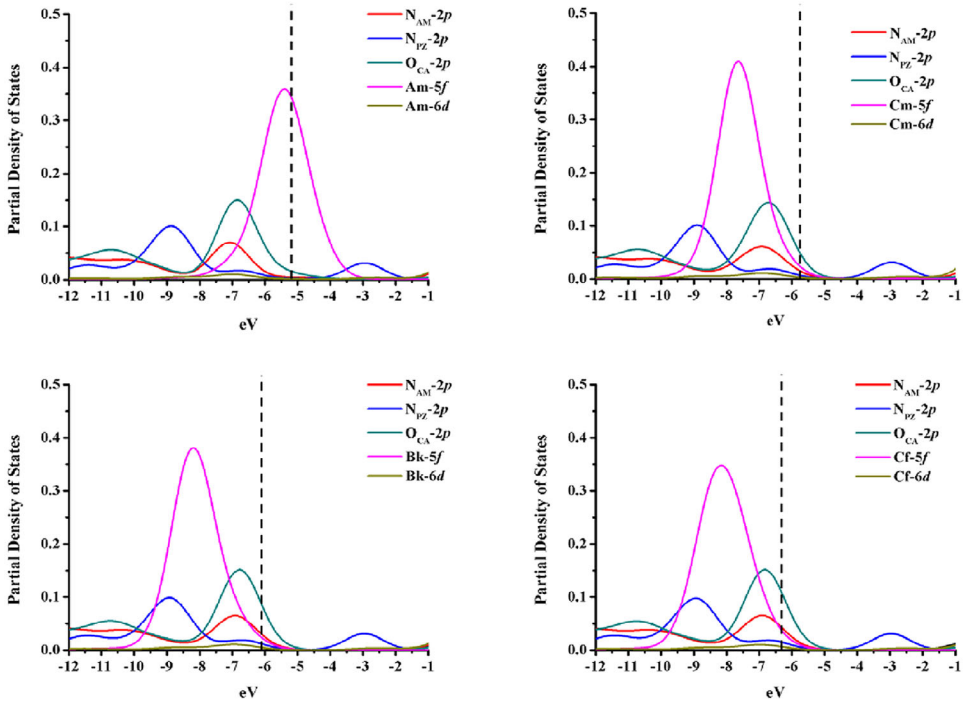

Figure 6. Partial density of states (PDOS) for $AnL^{2pz}(NO_3)(H_2O)$ complexes computed at the M06-L/6–311 + G(2df,p)/RECP level.

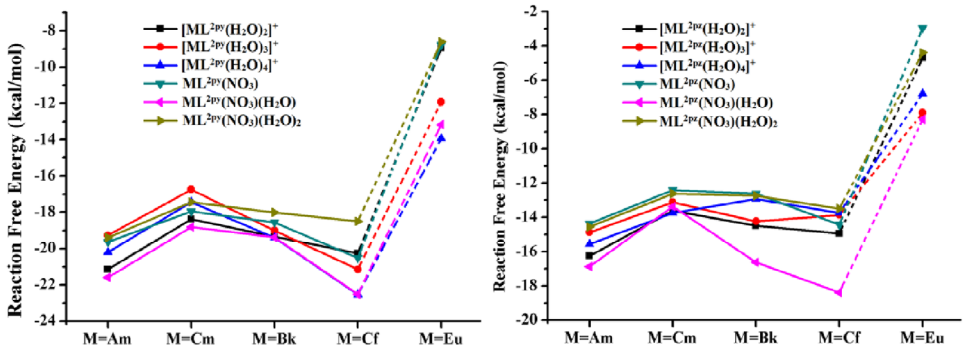

Figure 7. Changes in reaction free energy (ΔG, kcal/mol) for model back-extraction from M(*DEHP)$_3$(*HDEHP)$_2$(*DMDOHEMA) (M = Am, Cm, Bk, Cf, and Eu) to six product types, mediated by H_2L^{2py} (left) and H_2L^{2pz} (right) in *n*-dodecane/water solution.

of model ligands with ethyl chains (denoted as *DMDOHEMA, *DEHP and *HDEHP, presented in Figure S5) were used to model DMDOHEMA and HDEHP ligands, the model metal complexes M(*DEHP)$_3$(*HDEHP)$_2$-(*DMDOHEMA) after optimization were presented in Figure S6.

To investigate the thermodynamics of complex back-extraction processes, we constructed probable reaction pathways starting from water-soluble ligands (H_2L^{2py} and H_2L^{2pz}) and model complexes (M(*DEHP)$_3$(*HDEHP)$_2$(*DMDOHEMA)), generating back-extraction products: $[M(L^i)(H_2O)_2]^+$, $[M(L^i)(H_2O)_3]^+$, $[M(L^i)(H_2O)_4]^+$, $M(L^i)(NO_3)$, $M(L^i)(NO_3)(H_2O)$, and $M(L^i)(NO_3)(H_2O)_2$ (M = Am, Cm, Bk, Cf, Eu; $L^i = L^{2py}$, L^{2pz}). The overall reaction free energy $\Delta G_{back\text{-}extr}$ was calculated as $\Delta G_{back-extr} = \sum_m G_{product-m} - \sum_n G_{reactant-n}$. Gibbs free energies for all species in solution were computed using the IEFPCM solvation model at the M06-L/6–311 + G(2df,p)/RECP level, evaluating solvent effects for both *n*-dodecane (modeling TPH diluent) and aqueous phases. Figure 7 presents the variation in reaction free energy ($\Delta G_{back\text{-}extr}$) across actinides and product types. Analysis reveals $\Delta G_{back\text{-}extr}$ for all modeled back-extraction reactions are negative, ranging from −2.95 to −22.53 kcal/mol. These moderately negative values indicate both water-soluble ligands (H_2L^{2py} and H_2L^{2pz}) exhibit favorable stripping efficiency for Am, Cm, Bk, and Cf. Reaction energies systematically decrease from Am to Cm, increase from Cm to Bk, and continue increasing from Bk to Cf. This decrease-increase progression corresponds to analogous trends in ligand stripping capacity and agrees quantitatively with prior effective bond length and bonding analyses results. $\Delta G_{back\text{-}extr}$ values for H_2L^{2py} are ~4 kcal/mol more negative than comparative reactions with H_2L^{2pz}. Hence that the H_2L^{2py} possesses a stronger stripping capacity than the H_2L^{2pz} ligand, which can consist with the above atomic charge, ESP, partial covalent analyses, and the experimental findings. In literature,[67] Heitzmann find that with 0.5 M ligand, 0.4 M citric acid, and 0.3 M HDEHP, 0.6 M DMDOHEMA, and pH = 3, H_2L^{2py} did have stronger affinity toward Am^{3+} (D_{Am} = 1.37) and Eu^{3+}(D_{Eu} = 49) ions than those of H_2L^{2pz} ligand (D_{Am} = 0.31, D_{Eu} = 13).

Figure 7 further indicates that back-extraction reactions generating neutral $M(L^i)(NO_3)$-(H_2O) complexes (see the following Reaction (1)) exhibit the most negative $\Delta G_{back\text{-}extr}$ values when initiated from M(*DEHP)$_3$(*HDEHP)$_2$(*DMDOHEMA) precursors.

$$M(*DEHP)_3(*HDEHP)_2(*DMDOHEMA)_{org} + H_2L^i{}_{aq} + NO_3^- + H_3O^+{}_{aq} \rightarrow M(L^i)(NO_3)(H_2O)_{aq} + *DMDOHEMA_{org} + 5*HDEHP_{org} \quad (1)$$

This suggests neutral $M(L^i)(NO_3)(H_2O)$ complexes are likely the predominant back-extraction products for both ligands (H_2L^{2py} and H_2L^{2pz}). For these primary reactions, we computed differences in $\Delta G_{back\text{-}extr}$ among metal ions (Am, Cm, Bk, Cf, Eu) to evaluate intra-actinide separation capabilities and An/Eu separation key performance. The calculated $\Delta\Delta G_{Am/Eu}$, $\Delta\Delta G_{M1/M2}$ (M1 and M2 are two different metal of Am, Cm, Bk, Cf, and Eu) values are presented in Table 5.

The calculated $\Delta\Delta G_{Am/Eu}$ values for H_2L^{2py} and H_2L^{2pz} (An = Am, Cm, Bk, Cf) are consistently negative, thermodynamically confirming both ligands' significant selectivity for back-extracting Am^{3+}, Cm^{3+}, Bk^{3+}, and Cf^{3+} over Eu^{3+}. Notably, $\Delta\Delta G_{Am/Eu}$ for H_2L^{2pz} (−8.60 kcal/mol) is more negative than for H_2L^{2py} (−8.42 kcal/mol), indicating superior Am/Eu separation efficiency by H_2L^{2pz}. This computational finding aligns with Heitzmann's experimental results: H_2L^{2py} achieves Am^{3+} back-extraction from HDEHP-DMDOHEMA organic phase with separation factor $SF_{Am/Eu}$ = 36, whereas H_2L^{2pz} exhibits higher selectivity ($SF_{Am/Eu}$ = 41). Thus, our calculations quantitatively reproduce H_2L^{2pz}'s enhanced separation capability. According to Table 5, the calculated $\Delta\Delta G_{Am/Cm}$, $\Delta\Delta G_{Bk/Cm}$, and $\Delta\Delta G_{Cf/Cm}$ values are all negative, indicating that both studied ligands may separate Am^{3+}, Bk^{3+} and Cf^{3+} from Cm^{3+}. Specifically, the magnitudes of $\Delta\Delta G_{Am/Cm}$, $\Delta\Delta G_{Bk/Cm}$, and $\Delta\Delta G_{Cf/Cm}$ range from one-fourth to one-third of the calculated $\Delta\Delta G_{Am/Eu}$. Theoretically, the separation factor between metal ions (M1,M2) can be estimated using $SF_{M1/M2} = e^{-\frac{\Delta\Delta G_{M1/M2}}{RT}}$.[68] Thus, the estimated $SF_{Am/Cm}$, $SF_{Bk/Cm}$, $SF_{Cf/Cm}$ values likely range from 2.45 to 3.45, corresponding to the fourth-root to cubic-root values of the experimental $SF_{Am/Eu}$ data (36 and 41).

4. Conclusion

In this work, we theoretically investigated metal complexes formed by four trivalent transplutonium ions (Am^{3+}, Cm^{3+}, Bk^{3+}, Cf^{3+}) and two water-soluble ethylenediamine carboxylate

Table 5. Computed free energies $\Delta G_{back\text{-}extr}$ (kcal/mol) and differences $\Delta\Delta G_{M1/M2}$ (kcal/mol) for Am^{3+}, Cm^{3+}, Bk^{3+}, Cf^{3+}, and Eu^{3+} in model back-extraction reactions (1), evaluated at the M06-L/6–311 + G (2df,p)/RECP level with *n*-dodecane/water solution system.

Product species	$\Delta G_{back\text{-}extr}$	$\Delta\Delta G_{Am/M}$	$\Delta\Delta G_{Cm/M}$	$\Delta\Delta G_{Bk/M}$	$\Delta\Delta G_{Cf/M}$
$Am(L^{2py})(NO_3)(H_2O)$	−21.59	–	2.78	2.21	−0.93
$Am(L^{2pz})(NO_3)(H_2O)$	−16.88	–	3.51	0.25	−1.51
$Cm(L^{2py})(NO_3)(H_2O)$	−18.81	−2.78	–	−0.57	−3.71
$Cm(L^{2pz})(NO_3)(H_2O)$	−13.37	−3.51	–	−3.26	−5.02
$Bk(L^{2py})(NO_3)(H_2O)$	−19.38	−2.21	0.57	–	−3.14
$Bk(L^{2pz})(NO_3)(H_2O)$	−16.63	−0.25	3.26	–	−1.76
$Cf(L^{2py})(NO_3)(H_2O)$	−22.52	0.93	3.71	3.14	–
$Cf(L^{2pz})(NO_3)(H_2O)$	−18.39	1.51	5.02	1.76	–
$Eu(L^{2py})(NO_3)(H_2O)$	−13.17	−8.42	−5.64	−6.21	−9.35
$Eu(L^{2pz})(NO_3)(H_2O)$	−8.28	−8.60	−5.09	−8.35	−10.11

ligands (H_2L^{2py} and H_2L^{2pz}). The optimized geometries of these complexes closely resemble each other across all four transplutonium ions. After deducting metal ion radii, the effective bond length between metal ions and all N_{AM} (d_{eff}(An—N_{AM})), most $N_{PY/PZ}$, O_{CA} exhibit a distinctive "increasing–decreasing" trend (rising from Am to Cm, then declining from Cm to Bk, and continuing to decrease toward Cf). This trend inversely correlates with a corresponding "downward–upward" variation in bond strength across Am-Cm-Bk-Cf series. Mayer bond order (MBO) analyses confirmed that bonding intensities undergo this downward-upward variation. MBO results further revealed that H_2L^{2py} ligand exhibits stronger affinity toward all studied ions than H_2L^{2pz}. QTAIM parameters (H and |V|/G) suggests that the An—O_{CA} and An—N_{AM} bonds have weak yet significantly varying partial covalent interactions, and the covalency intensity of all An—N_{AM} bonds and most An—$N_{PY/PZ}$, An—O_{CA} bonds in studied complexes also follow a decreasing trend from Am to Cm, then increase from Cm to Bk and Cf. Consequently, this intensity variation may originate from differing covalency extents between donor atoms and Am^{3+}/Cm^{3+}/Bk^{3+}/Cf^{3+} ions. Additional covalency descriptors (Delocalization index, DI) likewise confirm that partial covalent character changes in the downward-upward pattern, with Cm identified as the transition point.

Despite exhibiting marginally longer bond lengths (as well as d_{eff} (M—N_{AM})), N_{AM} atoms demonstrate stronger binding affinity than $N_{PY/PZ}$ atoms in *N*-heterocyclic rings. This enhanced interaction is potentially attributable to electrostatic influences from nearby deprotonated O_{CA} atoms, and consequently serve as dominant contributors to the ligands' mutual separation capabilities. Thermodynamic analysis revealed superior stripping efficiency for the H_2L^{2py} ligand relative to H_2L^{2pz}, whereas H_2L^{2pz} exhibits enhanced Am/Eu separation performance. The calculated $\Delta\Delta G_{Am/Cm}$, $\Delta\Delta G_{Bk/Cm}$, and $\Delta\Delta G_{Cf/Cm}$ values approximate one-fourth to one-third of the $\Delta\Delta G_{Am/Eu}$ magnitude for a given ligand, suggesting themodynamic separation factors $SF_{Am/Cm}$, $SF_{Bk/Cm}$, $SF_{Cf/Cm}$ likely reside within 2.45–3.45 range. Collectively, these findings indicate both ligands possess significant potential for mutual group separation of the four trivalent transplutonium ions. We anticipate our work will provide fundamental molecular-level insights for designing advanced water-soluble ligands targeting: (1) mutual separation of Am, Cm, Bk, and Cf, and (2)f-element lanthanide-actinide separations.

Author Contributions

P.-W.H.: Methodology; data curation; visualization; writing original draft; funding acquisition; supervision. P.R.: Formal analysis; funding acquisition. M.Q.: Formal analysis.

Acknowledgments

This work was supported by the National Natural Science Foundation of China (Nos. 22276175, 21906152, 22266001), the Research Fund of Zhejiang Provincial Education Department (Nos. Y201738897, kg20160513), Nanxun scholars program of ZJWEU(RC2022010686), and the Jiangxi Provincial Natural Science Foundation (No. 20224BAB203007)

Conflict of Interests

The authors declare no conflict of interest.

Data Availability Statement

The data that support the findings of this study are available from the corresponding author upon reasonable request.

Keywords: Co-extraction · Partial covalent · Reaction free energy · Stripping · Transplutonium ion

[1] Danish, U. R., E. Seyfettin, *Nucl. Eng. Tech.* **2022**, *54*, 1312-1320.
[2] B. Pan, T. S. Adebayo, R. L. Ibrahim, M. A. S. Al-Faryan, *Energy Environ.* **2022**, *34*, 2521-2543.
[3] R. Taylor, G. Mathers, A. Banford, *Prog. Nucl. Energ.* **2023**, *64*, 104837.

[4] T. A. Kurniawan, M. H. D. Othman, D. Singh, R. Avtar, G. H. Hwang, T. Setiadi, W. Lo, *Annals Nucl. Energ.* **2022**, *166*, 108736.
[5] K. L. Nash, M. Nilsson, in *Reprocessing and Recycling of Spent Nuclear Fuel* (Ed: R. Taylor), Elsevier, Cambridge **2015**.
[6] J. R. Roberto, M. Du, J. G. Ezold, S. L. Hogle, J. Moon, K. Myhre, K. P. Rykaczewski, *Eur. Phys. J. A* **2023**, *59*, 304.
[7] N. Bessen, Q. Yan, N. Pu, J. Chen, C. Xu, J. Shafer, *Inorg. Chem. Front.* **2021**, *8*, 4177–4185.
[8] Z. Wang, X. Dong, Q. Yan, J. Chen, C. Xu, *Anal. Chem.* **2022**, *94*, 7743–7746.
[9] R. M. Pallares, D. D. An, G. J.-P. Deblonde, B. Kullgren, S. S. Gauny, E. E. Jarvis, R. J. Abergel, *Chem. Sci.* **2021**, *12*, 5295–5301.
[10] Y. Sasaki, Y. Tsubata, Y. Kitatsuji, Y. Morita, *Chem. Lett.* **2013**, *42*, 91–92.
[11] Y. Wang, F. Li, Z. Xiao, C. Wang, Y. Liu, W. Shi, H. He, *RSC Adv.* **2023**, *13*, 3781–3791.
[12] G. Modolo, S. Nabet, *Sol. Extr. Ion Exch.* **2005**, *23*, 359–373.
[13] K. P. Carter, R. M. Pallares, R. J. Abergel, *Commun. Chem.* **2020**, *3*, 103.
[14] Y. Liu, C. Wang, Q. Wu, J. Lan, W. Wu, Z. Chai, W. Shi, *Inorg. Chem.* **2025**, *64*, 9549–9557.
[15] A. Zaitsevskii, *Phys. Chem. Chem. Phys.* **2015**,*17*, 24831–24836.
[16] M. L. Neidig, D. L. Clark, R. L. Martin, *Coord. Chem. Rev.* **2013**, *257*, 394–406.
[17] N. Kaltsoyannis, *Chem. Euro. J.* **2018**, *24*, 2815–2825.
[18] E. M. Archer, F. A. Pereiro, J. M. Riley, J. P. Brannon, E. B. Flynn, J. C. Gilhula, B. L. Huffman, J. A. Jackson, J. G. Knapp, B. N. Long, H. E. Mason, M. S. Mullis, S. A. Kozimor, J. C. Shafer, S. S. Galley, *Inorg. Chem. Front.* **2025**, https://doi.org/10.1039/D5QI01056J.
[19] J. Dognon, *Coord. Chem. Rev.* **2014**, *266–267*, 110–122.
[20] C. A. P. Goodwin, J. F. Corbey, *Inorg. Chem.* **2024**, *63*, 9355–9362.
[21] M. A. Silver, S. K. Cary, J. A. Johnson, R. E. Baumbach, A. A. Arico, M. Luckey, M. Urban, J. C. Wang, M. J. Polinski, A. Chemey, G. Liu, K. Chen, S. M. Van Cleve, M. L. Marsh, T. M. Eaton, L. J. Van De Burgt, A. L. Gray, D. E. Hobart, K. Hanson, L. Maron, F. Gendron, J. Autschbach, M. Speldrich, P. Kögerler, P. Yang, J. Braley, T. E. Albrecht-Schmitt, *Science* **2016**, *353*, 3762.
[22] M. J. Polinski, E. B. Garner, R. Maurice, N. Planas, J. T. Stritzinger, T. G. Parker, H. N. Cross, T. D. Green, E. V. Alekseev, S. M. Van Cleve, W. Depmeier, L. Gagliardi, M. Shatruk, K. L. Knappenberger, G. Liu, S. Skanthakumar, L. Soderholm, D. A. Dixon, T. E. Albrecht-Schmitt, *Nat. Chem.* **2014**, *6*, 387–392.
[23] Y. Liu, C. Wang, Q. Wu, J. Lan, Z. Chai, Q. Liu, W. Shi, *Inorg. Chem.* **2021**, *60*, 10267–10279.
[24] S. Cooper, N. Kaltsoyannis, *Dalton Trans.* **2021**, *50*, 1478–1485.
[25] S. Cooper, N. Kaltsoyannis, *Dalton Trans.* **2022**, *51*, 5929–5937.
[26] Y. Liu, C. Wang, Q. Wu, J. Lan, Z. Chai, W. Wu, W. Shi, *Inorg. Chem.* **2022**, *61*, 4404–4413.
[27] X. Yu, D. Sergentu, R. Feng, J. Autschbach, *Inorg. Chem.* **2021**, *60*, 17744–17757.
[28] S. Ggracia, G. Arrachart, C. Marie, S. Chapron, M. Miguirditchian, S. Pellet-Rostaing, *Tetrahedron* **2015**, *71*, 5321–5336.
[29] N. Boubals, C. Wagner, T. Dumas, L. Chanèac, G. Manie, P. Kaufholz, C. Marie, P. J. Panak, G. Modolo, A. Geist, P. Guilbaud, *Inorg. Chem.* **2017**, *56*, 7861–7869.
[30] J. Borrini, A. Favre-Reguillon, M. Lemaire, S. Gracia, G. Arrachart, G. Bernier, X. Hérès, S. Pellet-Rostaing, *Solv. Extr. Ion Exch.* **2015**, *33*, 224–235.
[31] M. Heitzmann, F. Bravard, C. Gateau, N. Boubals, C. Berthon, J. Pécaut, M. Charbonnel, P. Delangle, *Inorg. Chem.* **2009**, *48*, 246–256.
[32] M. Heitzmann, C. Gateau, L. Chareyre, M. Miguirditchian, M. Charbonnel, P. Delangle, *New J. Chem.* **2010**, *34*, 108–116.
[33] P. Huang, C. Wang, Z. Su, D. Jiang, J. Wang, Q. Wu, J. Lan, W. Shi, *Supramol. Mater.* **2025**, *4*, 100092.
[34] P. D'Angelo, F. Martelli, R. Spezia, A. Filipponi, M. A. Denecke, *Inorg. Chem.* **2013**, *52*, 10318–10324.
[35] N. Morales, E. Galbis, J. M. Martinez, R. R. Pappalardo, E. S. Marcos, *J. Phys. Chem. Lett.* **2016**, *7*, 4275–4280.
[36] M. J. Frisch, G. W. Trucks, H. B. Schlegel, G. E. Scuseria, M. A. Robb, J. R. Cheeseman, G. Scalmani, V. Barone, B. Mennucci, G. A. Petersson, H. Nakatsuji, M. Caricato, X. Li, H. P. Hratchian, A. F. Izmaylov, J. Bloino, G. Zheng, J. L. Sonnenberg, M. Hada, M. Ehara, K. Toyota, R. Fukuda, J. Hasegawa, M. Ishida, T. Nakajima, Y. Honda, O. Kitao, H. Nakai, T. Vreven, J. A. Montgomery Jr., J. E. Peralta, F. Ogliaro, M. Bearpark, J. J. Heyd, E. Brothers, K. N. Kudin, V. N. Staroverov, T. Keith, R. Kobayashi, J. Normand, K. Raghavachari, A. Rendell, J. C. Burant, S. S. Iyengar, J. Tomasi, M. Cossi, N. Rega, J. M. Millam, M. Klene, J. E. Knox, J. B. Cross, V. Bakken, C. Adamo, J. Jaramillo, R. Gomperts, R. E. Stratmann, O. Yazyev, A. J. Austin, R. Cammi, C. Pomelli, J. W. Ochterski, R. L. Martin, K. Morokuma, V. G. Zakrzewski, G. A. Voth, P. Salvador, J. J. Dannenberg, S. Dapprich, A. D. Daniels, O. Farkas, J. B. Foresman, J. V. Ortiz, J. Cioslowski, D. J. Fox, *Gaussian 09, Revision D.01*, Gaussian, Inc., Wallingford CT **2013**.
[37] K. Nakamura, T. Kurisaki, H. Wakita, T. Yamaguchi, *Acta Cryst. C* **1995**, *51*, 1559–1563.
[38] N. Sakagomi, Y. Yamada, T. Konno, K. Okamoto, *Inorg. Chim. Acta* **1999**, *288*, 7–16.
[39] Y. Zhao, D. G. Truhlar, *Theor. Chem. Acc.* **2008**, *120*, 215–241.
[40] P. W. Huang, C. Z. Wang, Q. Y. Wu, J. H. Lan, G. Song, Z. F. Chai, W. Q. Shi, *Phys. Chem. Chem. Phys.* **2018**, *20*, 14031–14039.
[41] C. Ebenezer, R. V. Solomon, *Comment Inorg. Chem.* **2024**, *44*, 385–459.
[42] G. Odonkor, S. O. Odoh, *Inorg. Chem.* **2025**, *64*, 11518–11528.
[43] X. Cao, M. Dolg, H. Stoll, *J. Chem. Phys.* **2003**, *118*, 487–496.
[44] X. Cao, M. Dolg, *J. Mol. Struct. (Theochem)* **2004**, *673*, 203–209.
[45] T. Lu, F. Chen, *J. Comput. Chem.* **2012**, *33*, 580–592.
[46] T. Lu, *J. Chem. Phys.* **2024**, *161*, 082503.
[47] E. Cancès, B. Mennucci, J. Tomasi, *J. Chem. Phys.* **1997**, *107*, 3032–3041.
[48] A. Klamt, C. Moya, J. Palomar, *J. Chem. Theory Comput.* **2015**, *11*, 4220–4225.
[49] T. Lu, F. Chen, *Acta Phys. Chim. Sin.* **2012**, *28*, 1–18.
[50] E. Kraka, D. Setiawan, D. Cremer, *J. Comput. Chem.* **2016**, *37*, 130–142.
[51] P. Huang, *ChemistrySelect* **2019**, *4*, 12368-12374.
[52] R. D. Shannon, *Acta Cryst. Section A* **1976**, *32*, 751-767.
[53] C. R. Wick, T. Clark, *J. Mol. Mod.* **2018**, *24*, 142.
[54] J. Pilme, E. Renault, F. Bassal, M. Amaouch, G. Montavon, N. Galland, *J. Chem. Theory Comput.* **2014**, *10*, 4830-4841.
[55] E. Espinosa, E. Molins, C. Lecomte, *Chem. Phys. Lett.* **1998**, *285*, 170–173.
[56] A. Srivastave, R. Mishra, B. D. Joshi, V. Gupta, P. Tandon, *Mol. Simul.* **2014**, *40*, 1099–1112.
[57] P. Huang, C. Wang, Q. Wu, J. Lan, G. Song, Z. Chai, W. Shi, *Phys. Chem. Chem. Phys.* **2018**, *20*, 1030–1038.
[58] Y.u. A. Ustynyuk, Y.u. M. Alyapyshev, V. A. Babain, N. A. Ustynyuk, *Russ. Chem. Rev.* **2016**, *85*, 917–942.
[59] C. Outeiral, M. A. Vincent, A. M. Pendás, P. L. A. Popelier, *Chem. Sci.* **2018**, *9*, 5517–5529.
[60] M. Miguirditchian, V. Vanel, C. Marie, V. Pacary, M. Charbonnel, L. Berthon, X. Hérès, M. Montuir, C. Sorel, M. Bollesteros, S. Costenoble, C. Rostaing, M. Masson, C. Poinssot, *Solv. Extr. Ion Exch.* **2020**, *38*, 365–387.
[61] G. Modolo, A. Wilden, A. Geist, D. Magnusson, R. Malmbeck, *Radiochim. Acta* **2012**, *100*, 715–725.
[62] K. Bell, C. Carpentier, M. Carrott, A. Geist, C. Gregson, X. Hérès, D. Magnusson, R. Malmbeck, F. McLachlan, G. Modolo, U. Müllich, M. Sypula, R. Taylor, A. Wilden, *Procedia Chem* **2012**, *7*, 392–397.
[63] J. M. Muller, C. Berthon, L. Couston, D. Guillaumont, R. J. Ellis, N. Zorz, J. Simonin, L. Berthon, *Hydrometallurgy* **2017**, *169*, 542–551.
[64] B. Gannaz, R. Chiarizia, M. R. Antonio, C. Hill, G. Cote, *Solv. Extr. Ion Exch.* **2007**, *25*, 313–337.
[65] M. Kaneko, H. Suzuki, T. Matsumura, *Inorg. Chem.* **2018**, *57*, 14513–14523.
[66] S. K. M. Ali, S. Pahan, A. Bhattacharyya, P. K. Mohapatra, *Phys. Chem. Chem. Phys.* **2016**, *18*, 9816–9828.
[67] P. W. Huang, C. Z. Wang, Q. Y. Wu, J. H. Lan, Z. F. Chai, W. Q. Shi, *Sep. Purif. Technol.* **2023**, *319*, 124030.
[68] P. J. Panak, A. Geist, *Chem. Rev.* **2013**, *113*, 1199.

Manuscript received: July 26, 2025
Revised manuscript received: August 21, 2025
Version of record online: ■■, ■■